Korean J. Chem. Eng., 32(5), 860-866 (2015)
DOI: 10.1007/s11814-014-0272-3

pISSN: 0256-1115
eISSN: 1975-7220

Effects of nitrogen and carbon doping on properties and photocatalytic activity of TiO_2-In_2O_3 composite

Chung-Hsin Wu*,†, Chao-Yin Kuo, Jui-Tai Wu*, Pui-Kwan Andy Hong***, Chih-Hao Lai*, and Wei-Yang Chung***

*Department of Chemical and Materials Engineering, National Kaohsiung University of Applied Sciences, 415 Chien Kung Road, Kaohsiung, Taiwan
**Department of Environmental and Safety Engineering, National Yunlin University of Science and Technology, 123 University Road, Sec. 3, Douliou, Yunlin, Taiwan
***Department of Civil and Environmental Engineering, University of Utah, Salt Lake City, UT, USA
(*Received 20 April 2014 • accepted 11 September 2014*)

Abstract—TiO_2-In_2O_3 (Ti-In) was synthesized by the sol-gel method and the composite was further doped with nitrogen and carbon to create Ti-In-N and Ti-In-C, respectively. The dye C.I. Reactive Red 2 (RR2) was used a model compound to be subjected to various composites and measured for removal by photocatalytic degradation and adsorption. Ti-In-N possessed a larger mean diameter than Ti-In-C, while the latter possessed a greater anatase content and surface area than the former. After N or C doping, the spectra of corresponding Ti-In-N and Ti-In-C showed absorption edges at longer wavelengths than the parent Ti-In. Ti-N-O and Ti-O-C bonds were found in Ti-In-N and Ti-In-C composites, respectively. Ti-In-N was more effective for RR2 photodegradation than Ti-In-C, and the Ti-In-C removed more RR2 by adsorption than Ti-In-N.

Keywords: TiO_2, In_2O_3, Nitrogen-doping, Carbon-doping, Photodegradation

INTRODUCTION

Semiconductor photocatalysts are commonly used to activate free-radical chain reactions of photocatalytic oxidation. TiO_2 has been most widely used because of its chemical stability and low toxicity. TiO_2 can be modified by doping with metals and nonmetals to reduce the band-gap energy, to extend the life and utility of photogenerated electron-hole pair, or to improve pollutant adsorption to the catalyst surface [1]. Several studies involving nitrogen-doped TiO_2 [2-5] and carbon-doped TiO_2 [6-8] showed a reduced band-gap energy as well as enhanced photocatalytic activity in the modified TiO_2.

Rodriguez-Gonzalez et al. [9] found doping of TiO_2 with In_2O_3 increased photocatalytic activity because of increased surface area of the catalyst. Wu et al. [10] attributed an increased photocatalytic activity of TiO_2-In_2O_3 composite (Ti-In) to an increased surface area as measured by BET, as well as to increased hydrophilicity and separation of photogenerated electron-hole pairs afforded by the modified catalyst. Other studies involving Ti-In synthesized by the sol-gel method also concluded in enhanced removal of organic contaminants by Ti-In over the original TiO_2 [10-12]. Ma et al. [13] doped Ti-In with Pt and found resulting photocatalytic activities in the order of Pt/Ti-In>Ti-In>TiO_2. With a strong ability to accommodate conduction-band electrons, the incorporated Pt enhanced the overall photocatalytic activity via improved charge separation of the photogenerated electron-hole pairs. Sojic et al. [14] found nonmetal dopants to be more effective than metal dopants. However, to the best of our knowledge, photocatalytic activities of Ti-In with nitrogen and carbon dopants have not been examined. This study synthesized the Ti-In photocatalyst via the sol-gel method, doped it with N and C separately, and characterized the surface properties of the resulting catalyst. To examine the photocatalytic activities of N-doped and C-doped Ti-In, the removal of a common azo dye C.I. Reactive Red 2 (RR2) was studied. Our project objectives were to (i) prepare an N-doped Ti-In (abbreviated as Ti-In-N) and a C-doped Ti-In (Ti-In-C) with varied Ti/N and Ti/C mole ratios, (ii) characterize the surface properties of various Ti-In-N and Ti-In-C, (iii) determine adsorptive changes of RR2 onto Ti-In-N and Ti-In-C, and (iv) assess the photocatalytic activities in decolorizing RR2 of the doped Ti-In-N and Ti-In-C relative to their parent Ti-In.

MATERIALS AND METHODS

1. Materials

RR2 ($C_{19}H_{10}Cl_2N_6Na_2O_7S_2$) was purchased from Sigma Aldrich. $TiCl_4$ (Acros) and $InCl_3$ (Alfa Aesar) were sources of Ti and In, respectively. Urea (Katayama) and powder activated carbon (PAC) (Katayama) were sources of N and C dopants, respectively. The solution pH was adjusted by adding 0.1 M HNO_3 (Merck) or NaOH (Merck) during reaction. All compounds were used as received without purification.

2. Preparation of Ti-In, Ti-In-N, and Ti-In-C

Ti-In was prepared in Ti/In mole ratio of 54 by the sol-gel method as previously described [10]. The N-doped TiO_2-In_2O_3 is denoted

†To whom correspondence should be addressed.
E-mail: wuch@kuas.edu.tw

as Ti-In-N-# where # represents the Ti/N mole ratio, and the C-doped TiO_2-In_2O_3 is likewise denoted as Ti-In-C-# where # is the Ti/C mole ratio. To prepare the Ti-In-N-0.07 catalyst, Ti-In (2.5 g) and urea (12.5 g) were thoroughly mixed and the mixture was calcined at 450 °C for 2 h. Ti-In-N-0.06 and Ti-In-N- 0.18 were similarly prepared by varied urea amounts. To prepare the Ti-In-C-13.3 catalyst, PAC (0.104 g) was first mixed with HCl (20 mL; 0.65 M) by placing the mixture in an ultrasonic bath for 10 min; then to this solution $InCl_3$ (0.943 g; 99.9%) and $TiCl_4$ (6.7 mL; 98%) were added. The solution pH was adjusted to pH 8 by adding an NH_4OH solution (28%), resulting in formation of a solid precipitate. The precipitate was collected by filtration and washed repeatedly with distilled water; it was dried at 110 °C for 24 h and then calcined at 450 °C for 2 h to yield the Ti-In-C-13.3 catalyst. Ti-In-C-2.7 and Ti-In-C-5.3 were prepared similarly by varying the PAC amount. Since C-N co-doped Ti-In (Ti-In-C-N at Ti/N=0.07 and Ti/C=13.3) will be generated and evaluated in our future studies, Ti-In-N-0.07 and Ti-In-C-13.3 were selected as the representative samples for N- and C-doped Ti-In in this study.

3. Characterization of Photocatalysts

The crystalline structures of various photocatalysts were analyzed by X-ray diffraction (XRD) (Bruker D8 SSS, Germany). The XRD patterns were recorded with 2θ values of 10-90°, with accelerating voltage and applied current of 40 kV and 30 mA, respectively. The pH point of zero charge (pH_{pzc}) of particles was determined in the range of 3-10 using a Zeta-Meter 3.0 (USA). The morphologies and structures of the prepared Ti-In-N and Ti-In-C were characterized using a JEOL 3010 (Japan) transmission electron microscope (TEM). Diffuse reflectance UV-Vis spectra of the photocatalysts were obtained using a UV-Vis spectrophotometer (JAS.CO-V670, Japan) and were used to calculate the band-gap energies. The specific surface areas of samples were calculated from nitrogen adsorption isotherms by BET method using a Micromeritics ASAP 2020 apparatus. X-ray photoelectron spectroscopy (XPS) measurements were made by using a PHI Quantum 5000 XPS system (USA) with a monochromatic Al Kα source and a charge neutralizer.

4. Photodegradation and Adsorption of RR2

Experiments were conducted with each photocatalyst of 0.2 g/L at pH 3 and 25 °C. RR2 of 20 mg/L was used in all experiments except those varied to determine the concentration effect of RR2 on its decolorization. Decolorization experiments were in a 3-L hollow cylindrical glass reactor, illuminated by an 8-W UV lamp (254 nm, Philips) with light intensity of 1.12 W/m^2 that was placed inside a quartz tube. Adsorption experiments were performed in the dark. The reaction medium was continuously stirred at 300 rpm to maintain it in suspension. Aliquots, a total volume of 10 mL, were withdrawn from the reactor at time intervals to monitor reaction progress. Following sampling, solids were separated by filtration through a 0.22 μm filter (Millipore), and RR2 remaining in the filtrate was analyzed by absorbance at 538 nm with a spectrophotometer (Hitachi U-5100, Japan).

RESULTS AND DISCUSSION

1. Surface Characteristics of Photocatalysts

Fig. 1 shows the XRD patterns of Ti-In-N and Ti-In-C. The 2θ peaks at 25.4° and 48.1° were associated with anatase TiO_2 and those at 27.5°, 36.2°, 41.3° and 54.4° with rutile TiO_2. No patterns included any In_2O_3, N-derived, or C-derived peaks. Wu et al. [10] suggested that the absence of In_2O_3 peaks from Ti-In was due to its significant dispersion in Ti-In at low level (Ti/In mole ratio of 54) and its low crystallinity in Ti-In to be measurable by XRD. Previous investigations were unable to observe N-derived peaks for N-doped TiO_2 [5] or C-derived peaks for the TiO_2/PAC composite [8].

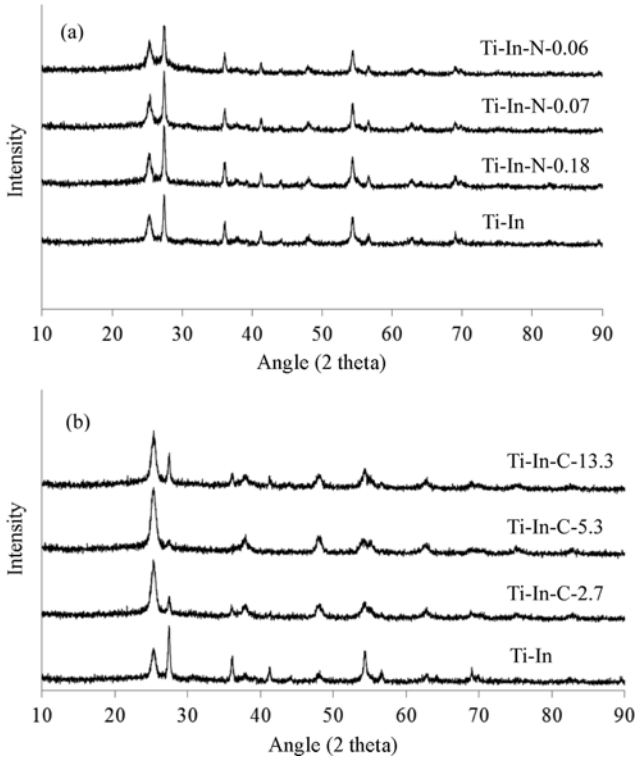

Fig. 1. XRD patterns measured of prepared composites of (a) Ti-In-N and (b) Ti-In-C.

The anatase content was determined from integrated intensity of anatase diffraction peak at 2θ=25.4°, I_A, and the rutile content from rutile diffraction peak at 2θ=27.5°, I_R, using Eq. (1) below [15]. Based on the XRD patterns, the crystalline size was calculated using Eq. (2) per Scherrer [16]:

$$\text{Anatase}(\%) = \frac{1}{1+12.6\frac{I_A}{I_R}} \times 100 \quad (1)$$

$$D = \frac{0.9\lambda}{\beta\cos\theta} \quad (2)$$

where D represents the crystalline size (nm), λ the X-ray wavelength (0.15418 nm), β the line-width at half maximum of anatase peak at 2θ=25.4° or of rutile peak at 2θ=27.5°, and θ the diffraction angle (°). Table 1 lists crystalline percentages and diameters of the composites. The crystalline percentage of anatase and mean diameter of Ti-In were similar to those of Ti-In-N, because crystalline growth of Ti-In reached completion during the sol-gel and calcination processes. Additionally, Ti-In was used to create

Table 1. Crystalline contents and diameters of prepared composites

Photocatalyst	Crystalline (%)		Diameter (nm)		Mean diameter (nm)
	Anatase	Rutile	Anatase	Rutile	
Ti-In	30	70	25	71	57
Ti-In-N-0.06	31	69	17	60	47
Ti-In-N-0.07	27	73	17	68	54
Ti-In-N-0.18	27	73	17	70	56
Ti-In-C-13.3	57	43	13	79	41
Ti-In-C-5.3	85	15	25	40	27
Ti-In-C-2.7	77	23	13	54	22

Table 2. Band-gap energies and BET surface areas of prepared composites

Photocatalyst	Wavelength (nm)	Band-gap energy (eV)	BET surface area (m^2/g)
Ti-In	418	2.97	35.7
Ti-In-N-0.06	431	2.88	22.0
Ti-In-N-0.07	432	2.87	30.5
Ti-In-N-0.18	429	2.89	31.8
Ti-In-C-13.3	426	2.91	60.6
Ti-In-C-5.3	438	2.83	77.9
Ti-In-C-2.7	464	2.67	131

Ti-In-N through a post-nitridation route. Therefore, Ti-In and Ti-In-N did not differ significantly in crystalline percentages and diameters. The XRD figures reveal that C doping retarded the transformation of the TiO_2 from anatase to rutile, leaving a higher content of anatase than rutile in Ti-In-C. The suppressed phase transformation might have resulted from stabilization of the anatase phase by the surrounding PAC. The presence of PAC inhibited TiO_2 aggregation during calcination, resulting in reduced particle size after C doping (Table 1). Wang et al. [17] and Slimen et al. [7] showed that activated carbon suppressed the growth of TiO_2 powder and prevented agglomeration. Ti-In-N showed a larger mean diameter than Ti-In-C, while the latter a higher anatase content (Table 1).

The pH_{pzc} values of Ti-In, Ti-In-N-0.07, and Ti-In-C-13.3 were 4.9, 4.8, and 5.3, respectively. In experiments at pH 3, the catalyst surfaces were positively charged. Table 2 presents the band-gap energies and BET surface areas of the prepared catalysts. The spectra of Ti-In-N and Ti-In-C show absorption edges at longer wavelengths than their parent Ti-In, suggesting reduced band-gap energies of Ti-In-N and Ti-In-C after doping. This red shift means the doped photocatalysts can be excited by photons of lower energy to generate reactive hole-electron pairs, possibly leading to enhanced photocatalytic activity. Ti-In-C had a higher surface area than its parent Ti-In, because dopant PAC had a high surface area (968 m^2/g). The surface areas followed the order of Ti-In-C>Ti-In>Ti-In-N. Therefore, doping with PAC increased the surface area and reduced both the diameter and band-gap energy of the parent Ti-In particles.

A common perception in TiO_2 photocatalysis literature is that the anatase phase is more photoactive than the rutile phase; however, this is not always true. Aside from the bulk structure of the former, the most important difference between anatase and rutile is band-gap energy. The general consensus is that the band gaps of rutile and anatase TiO_2 are 3.03 and 3.20 eV, respectively [18]. Rutile TiO_2 had higher water oxidation photocurrent under simulated sunlight than UV, so the photocatalytic activity of anatase and rutile can differ depending on the type of chemicals. Hurum et al. [19] indicated that electron-trapping sites are more stable in anatase than in rutile, so anatase exhibits greater photocatalytic activity. Theoretically, increasing the amount of anatase to rutile in doped Ti-In increased the band-gap energy and the photocatalytic activity of photocatalyst. However, Henderson [20] claimed that the mixed-phase TiO_2 exhibited higher photoactivity than single-phase TiO_2; moreover, the optimal anatase content in mixed-phase TiO_2 depended on the method of preparation and the photocatalytic reaction of interest. The binding energy of the valence band of anatase

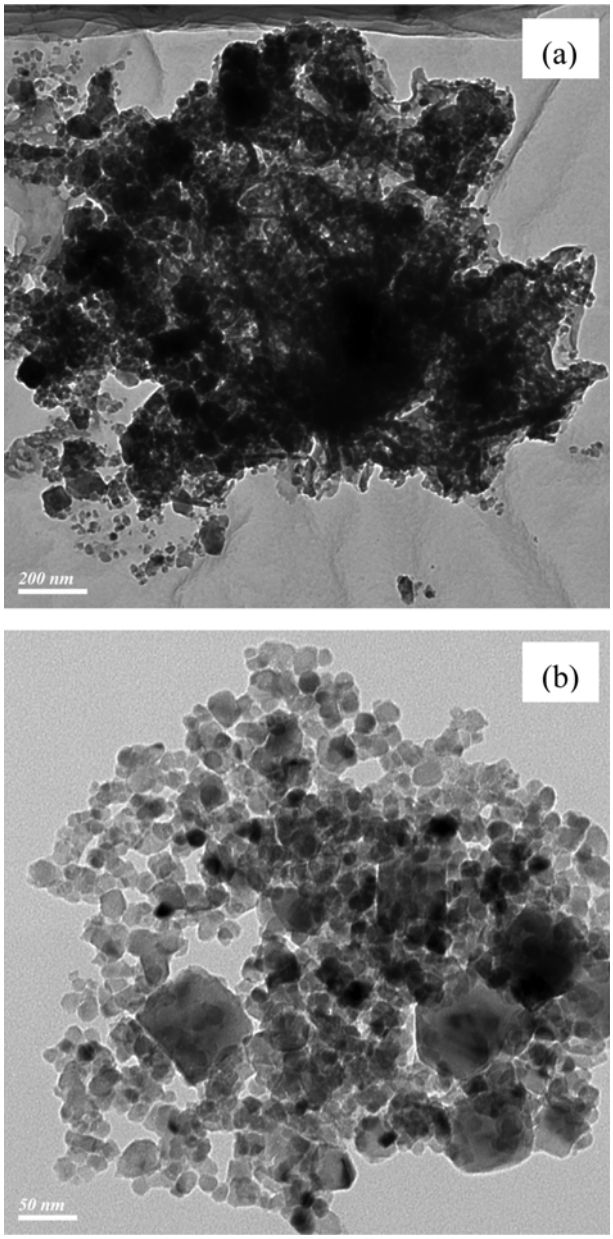

Fig. 2. TEM micrographs of (a) Ti-In-N-0.07 and (b) Ti-In-C-13.3.

was found to be 0.39 eV higher than that of rutile in composite samples. In mixed anatase/rutile samples, electrons have been demonstrated to flow from rutile into anatase, and holes have been shown to move oppositely [18]. Accordingly, mixed anatase/rutile samples exhibit a better photocatalytic activity than single anatase (or rutile) samples.

Changes in particle size affect photoactivity by changing surface area, light scattering and light absorptivity. These factors can work together or against each other in photocatalytic reactions. Benko et al. [21] proposed that charge carrier injection and/or trapping at particle surface sites depends on a particle's size: larger particles exhibit more stable surface sites for electron trapping. Large surface areas facilitate contact between holes (or electrons) and pollutant molecules, improving photocatalytic activities. However, it is difficult to accurately compare different photocatalysts due to particle size and surface area differences and lack of knowledge regarding what fraction of a nanoparticle's surface is active.

TEM offers insight into the morphology and microstructure of the photocatalysts. The TEM images in Fig. 2 display the structures of Ti-In-N-0.07 and Ti-In-C-13.3. A wormhole-like mesoporous structure was observed at the edges of the TEM images of both Ti-In-N-0.07 and Ti-In-C-13.3. The mesopores formed by aggregation of nanoparticles were of several nanometers. The aggregates of Ti-In-N-0.07 and Ti-In-C-13.3 were of 50-100 and 20-50 nm, respectively.

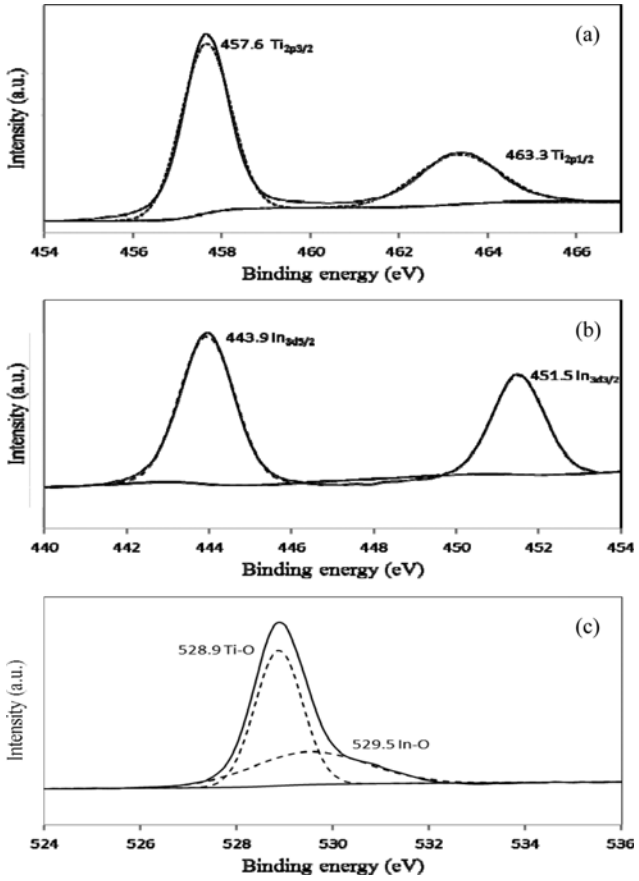

Fig. 3. XPS spectra of Ti-In (a) Ti_{2p}, (b) In_{3d}, (c) O_{1s} [10].

XPS was used to determine the chemical compositions of the photocatalysts. Figs. 3(a)-(c) present the XPS spectra of Ti_{2p}, In_{3d}, and O_{1s}, respectively, for Ti-In. Figs. 4(a)-(d) present the XPS spectra of Ti_{2p}, In_{3d}, N_{1s}, and O_{1s}, respectively, for Ti-In-N-0.07. Figs. 5(a)-

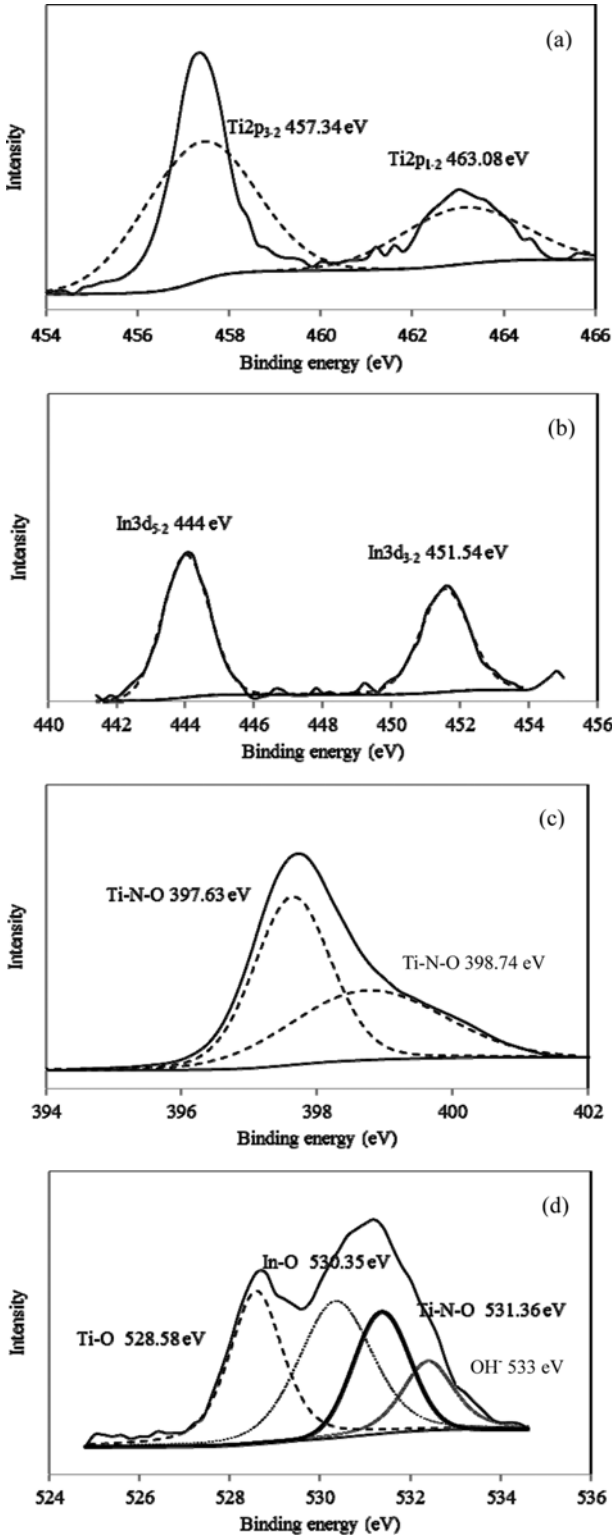

Fig. 4. XPS spectra of Ti-In-N-0.07 for (a) Ti_{2p}, (b) In_{3d}, (c) N_{1s}, and (d) O_{1s}.

(d) show the XPS spectra of Ti_{2p}, In_{3d}, C_{1s}, and O_{1s}, respectively, for Ti-In-C-13.3. $Ti_{2p3/2}$ and $Ti_{2p1/2}$ spin-orbital splitting photoelectrons were located at binding energies of 455.7-458.8 and 462.1-464.5 eV [22-24], respectively (Figs. 3(a), 4(a) and 5(a)). These binding energies are close to reported values for Ti^{4+} in TiO_2 [25]. $In_{3d5/2}$ and $In_{3d3/2}$ spin-orbital splitting photoelectrons were observed at binding energies of 443.9-445 [23,26-29] and 451.5-452.2 eV [23,26,27, 29], respectively (Figs. 3(b), 4(b) and 5(b)).

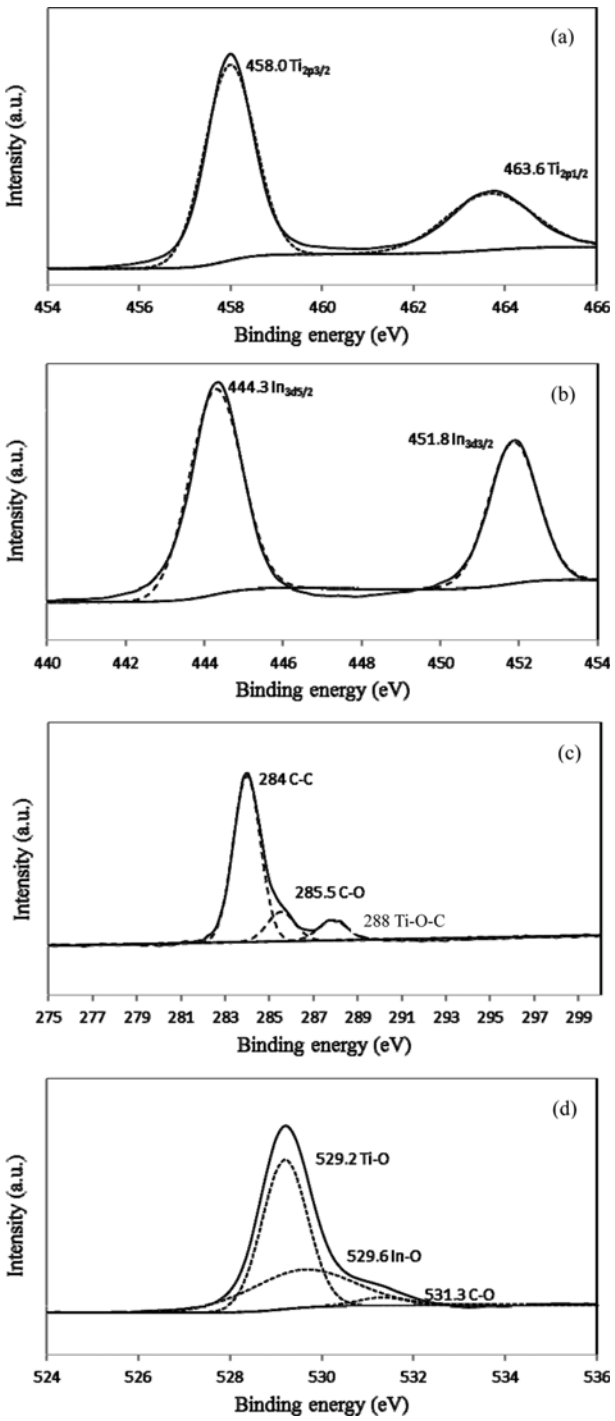

Fig. 5. XPS spectra of Ti-In-C-13.3 for (a) Ti_{2p}, (b) In_{3d}, (c) C_{1s}, and (d) O_{1s}.

Two peaks with binding energies of 397.6 and 398.7 eV were identified in the N_{1s} region of Ti-In-N-0.07 (Fig. 4(c)). Binding energies of 397.0-397.4 [30-32] and 398.6 eV [30,31] in the N_{1s} region were assigned to Ti-N-O. Asahi et al. [2] proposed that nitrogen doped at the substitutional sites of TiO_2 in N-TiO_2; however, Reyes-Garcia et al. [33] claimed that nitrogen atoms doped at the interstitial sites. Peaks of the N_{1s} region at 396-397 eV were attributed to substitutional nitrogen owing to the closeness of this region to the typical binding energy of 396 eV that has been observed for N in TiN, while observed peaks at higher binding energies are usually ascribed to a generic interstitial site [34]. Furthermore, analysis of the interaction between nitrogen impurities and oxygen vacancies has demonstrated that interstitial sites are more stable than substitutional sites in N-TiO_2 [34]. Two peaks with binding energies of 397.6 and 398.7 eV were assigned to Ti-N-O, and the nitrogen atoms were suggested herein to occupy interstitial positions in Ti-In-N. Peaks at 528.5-529.2 [23,24,35] and 529.4-530.0 eV [22,27, 28] were assigned to O_{1s}; the former was attributable to Ti-O and the latter to In-O (Figs. 3(c), 4(d) and 5(d)). Peaks at 531.4 and 533 eV indicated other oxygen species, plausibly belonging to Ti-N-O [32] and OH^- [22], respectively (Fig. 4(d)). The binding energies of C_{1s}, 284.8, 285.4 and 288 eV, were attributed to C-C, C-O [36,37], and Ti-O-C [22] bonds, respectively (Fig. 5(c)). The peak of O_{1s} at 530.7-531.2 eV was attributed to oxygen associated with C-O contamination [27] (Fig. 5(d)). XPS characterization thus confirmed that Ti-N-O and Ti-O-C had been formed in Ti-In-N-0.07 and Ti-In-C-13.3, respectively.

2. Photocatalytic Activity of Prepared Composites

Fig. 6 presents the effects of N and C dopant concentrations in Ti-In on RR2 removal. After 180 min, the adsorptions of RR2 (in the dark) by Ti-In, Ti-In-N-0.06, Ti-In-N-0.07, Ti-In-N-0.18, Ti-In-C-2.7, Ti-In-C-5.3, and Ti-In-C-13.3 were 34%, 11%, 20%, 25%, 80%, 72%, and 64%, respectively, while the total removals of RR2 (adsorption and photodegradation under illumination) were 78%, 97%, 98%, 96%, 95%, 90%, and 92%, respectively. Therefore, the net removal of RR2 attributed to photodegradation by various photocatalysts followed the order of Ti-In-N-0.06>Ti-In-N-0.07>Ti-In-N-0.18>Ti-In>Ti-In-C-13.3>Ti-In-C-5.3>Ti-In-C-2.7. Both the surface area of Ti-In-N (Table 2) and its adsorption of RR2 (Fig. 6(a)) decreased as N doping increased; however, the net photodegradation of RR2 increased with increasing N doping. The removal of RR2 in all experiments followed pseudo-first-order kinetics, as has been reported in various studies of dye decolorization [8,10,38,39]. Table 3 lists the fitted pseudo-first-order rate constants along with correlation coefficients for various photocatalysts. Nitrogen doping greatly improved photocatalytic activity of Ti-In. Xing et al. [40] showed that doping of nitrogen into the TiO_2 lattice improved its photocatalytic activity, but adsorption of nitrogen onto the TiO_2 surface hindered it.

Both the surface area of Ti-In-C (Table 2) and its adsorption of RR2 (Fig. 6(b)) increased with increasing C doping; however, the net photodegradation of RR2 decreased as C doping increased. The distribution of TiO_2 on PAC particles might enhance charge transfer between TiO_2 and PAC, thereby improving the photocatalyst's ability to absorb light. However, Ti-In-C did not exhibit this effect. The results suggested that PAC in Ti-In-C assisted in adsorption of

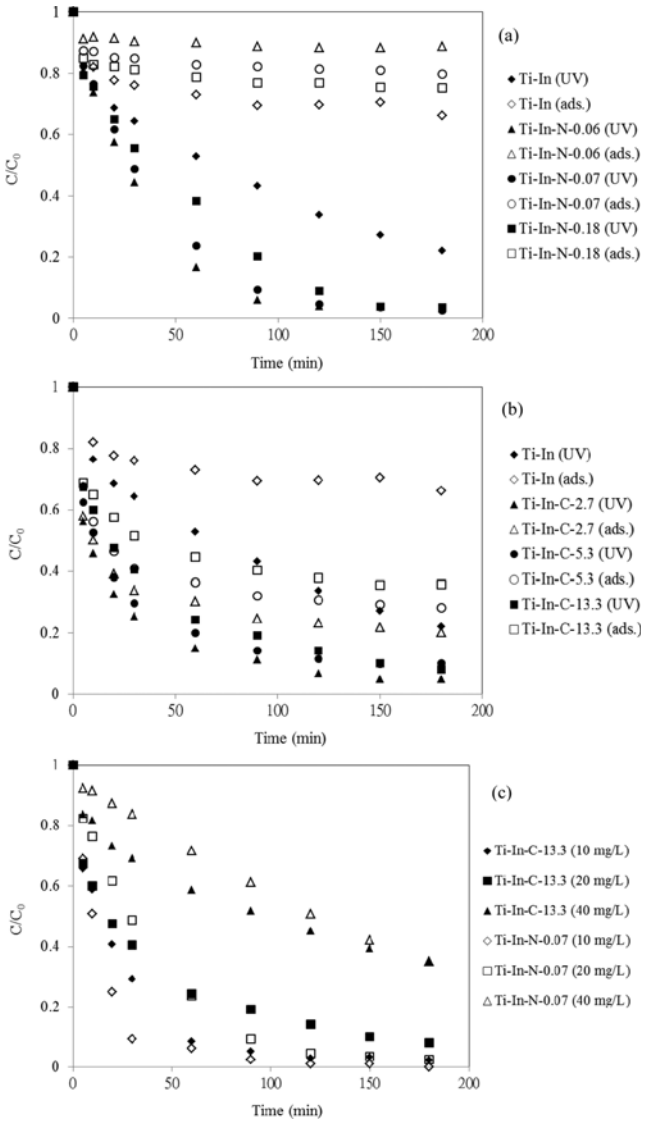

Fig. 6. Removal of RR2 under different conditions: (a) N-doping concentrations, (b) C-doping concentrations, and (c) initial RR2 concentrations.

the contaminant dye but it did not prove to be an efficient accepter of photogenerated electrons as to prevent recombination. The removal of RR2 by Ti-In-N was higher than by Ti-In-C (Table 3).

Fig. 6(c) shows the effect of RR2 concentration on its decolorization by UV/Ti-In-C-13.3 and UV/Ti-In-N-0.07. After 180 min, the removals of RR2 from initial concentrations of 10, 20, and 40 mg/L by UV/Ti-In-C-13.3 were 98%, 92%, and 65%, respectively; whereas the removals from the same set of initial concentrations by UV/Ti-In-N-0.07 were 100%, 98%, and 65%, respectively. The removal of RR2 at 180 min decreased as the initial RR2 concentration increased, which suggested the reaction order with respect to RR2 was not first-order over the studied concentration range. The varying rate constant k_1 (as shown in Table 3) according to varying initial RR2 concentration again reflected that the reaction was not first-order, albeit the fitted k_1 rate constants still provided kinetic comparison among the catalysts under the same conditions. Clearly,

Table 3. Pseudo-first-order rate constant (k) of removal and correlation coefficient (R^2) in various operation systems ([RR2] =20 mg/L, [photocatalyst]=0.2 g/L, pH=3)

Systems	k (h^{-1})	R^2
UV/Ti-In	0.43	0.999
UV/Ti-In-N-0.06	1.7	0.988
UV/Ti-In-N-0.07	1.6	0.997
	2.0*	0.938*
	0.34**	0.997**
UV/Ti-In-N-0.18	1.1	0.978
UV/Ti-In-C-13.3	0.76	0.979
	1.7*	0.975*
	0.29**	0.991**
UV/Ti-In-C-5.3	0.860	0.941
UV/Ti-In-C-2.7	0.960	0.971

*Denotes values for [RR2]=10 mg/L
**Denotes values for [RR2]= 40 mg/L

other factors such as the extent of adsorption or photon reception at the catalyst surface might have played a role in the observed reaction order on RR2. With increased RR2 concentration, it would to some extent shield the photocatalytically active sites from a given photon flux, resulting in reduced contaminant conversion. In addition, the increasing amount of RR2 and correspondingly of intermediates could have resulted in stronger competition for the photogenerated hydroxyl radicals. Thus, for the same amounts of photocatalyst and photon input toward an increased RR2 load, the removal of contaminant could be reduced due to shielding or increased consumption of hydroxyl radical. Similar reduced activities were found in numerous studies of UV/TiO_2 system [38,41].

CONCLUSIONS

Ti-In, Ti-In-N and Ti-In-C were prepared and their surface characteristics and photocatalytic activities were measured. Doping Ti-In with nitrogen or carbon reduced the band-gap energy of Ti-In. Surface areas of the three followed the order of Ti-In-C>Ti-In>Ti-In-N. XPS characterization verified that Ti-N-O and Ti-O-C bonds were formed in Ti-In-N and Ti-In-C, respectively. PAC in Ti-In-C improved adsorption capacity for RR2 but did not trap photogenerated electrons or improve photodegradation. Ti-In-N removed RR2 via photocatalytic degradation more effectively than Ti-In-C did, while the latter removed more RR2 by adsorption than the former.

ACKNOWLEDGEMENTS

The authors would like to thank the National Science Council of the Republic of China, Taiwan, for financially supporting this research under Contract No. NSC 101-2221-E-151-038-MY3.

REFERENCES

1. S. H. S. Chan, T. Y. Wu, J. C. Juan and C. Y. Teh, *J. Chem. Technol. Biotechnol.*, **86**, 1130 (2011).

2. R. Asahi, T. Morikawa, T. Ohwaki, K. Aoki and Y. Taga, *Science*, **293**, 269 (2001).
3. R. Silveyra, L. T. Saenz, W. A. Flores, V. C. Martınez and A. A. Elguezabal, *Catal. Today*, **107-108**, 602 (2005).
4. Y. Ma, J. Zhang, B. Tian, F. Chen and L. Wang, *J. Hazard. Mater.*, **182**, 386 (2010).
5. C. H. Wu, C. Y. Kuo, C. J. Lin and P. K. Chiou, *Int. J. Photoenergy*, **2013**, Article ID 439079 (2013).
6. B. Gao, P. S. Yap, T. M. Lim and T. T. Lim, *Chem. Eng. J.*, **171**, 1098 (2011).
7. H. Slimen, A. Houas and J. P. Nogier, *J. Photochem. Photobiol. A: Chem.*, **221**, 13 (2011).
8. C. Y. Kuo, C. H. Wu and S. T. Chen, *Desalin. Water Treat.*, **52**, 834 (2014).
9. V. Rodriguez-Gonzalez, A. Moreno-Rodriguez, M. May, F. Tzompantzi and R. Gomez, *J. Photochem. Photobiol. A Chem.*, **193**, 266 (2008).
10. C. H. Wu, C. Y. Kuo, C. H. Lai and W. Y. Chung, *React. Kinet. Mech. Catal.*, **112**, 543 (2014).
11. D. Shchukin, S. Poznyak, A. Kulak and P. Pichat, *J. Photochem. Photobiol. A Chem.*, **162**, 423 (2004).
12. L. C. Chen, C. M. Huang, C. S. Gao, G. W. Wang and M. C. Hsiao, *Chem. Eng. J.*, **175**, 49 (2011).
13. F. Ma, S. Zhang, X. Yang, W. Guo, Y. Guo and M. Huo, *Catal. Commun.*, **24**, 75 (2012).
14. D. V. Sojic, V. N. Despotovic, N. D. Abazovic, M. I. Comor and B. F. Abramovic, *J. Hazard. Mater.*, **179**, 49 (2010).
15. R. A. Spurr and H. Myers, *Anal. Chem.*, **29**, 760 (1957).
16. P. Klug and L. E. Alexander, *X-ray diffraction procedures*, Wiley, New York (1974).
17. Y. Wang, M. Zhong, F. Chen and J. Yang, *Appl. Catal. B: Environ.*, **90**, 249 (2009).
18. D. O. Scanlon, C. W. Dunnill, J. Buckeridge, S. A. Shevlin, A. J. Logsdail, S. M. Woodley, C. R. A. Catlow, M. J. Powell, R. G. Palgrave, I. P. Parkin, G. W. Watson, T. W. Keal, P. Sherwood, A. Walsh and A. A. Sokol, *Nat. Mater.*, **12**, 798 (2013).
19. D. C. Hurum, A. G. Agrios, K. A. Gray, T. Rajh and M. C. Thurnauer, *J. Phys. Chem. B*, **107**, 4545 (2003).
20. M. A. Henderson, *Surf. Sci. Rep.*, **66**, 185 (2011).
21. G. Benko, B. Skarman, R. Wallenberg, A. Hagfeldt, V. Sundstrom and A. P. Yartsev, *J. Phys. Chem. B*, **107**, 1370 (2003).
22. Q. Xiao and L. Ouyang, *Chem. Eng. J.*, **148**, 248 (2009).
23. R. Sasikala, A. R. Shirole, V. Sudarsan, Jagannath, C. Sudakar, R. Naik, R. Rao and S. R. Bharadwaj, *Appl. Catal. A: Gen.*, **377**, 47 (2010).
24. X. Wang and T. T. Lim, *Appl. Catal. A: Gen.*, **399**, 233 (2011).
25. X. Wang, Z. Hu, Y. Chen, G. Zhao, Y. Liu and Z. Wen, *Appl. Surface Sci.*, **255**, 3953 (2009).
26. S. K. Poznyak, A. N. Golubev and A. I. Kulak, *Surf. Sci.*, **454-456**, 396 (2000).
27. M. Tominaga, N. Hirata and I. Taniguchi, *Electrochem. Commun.*, **7**, 1423 (2005).
28. K. R. Reyes-Gil, E. A. Reyes-Garcia and D. Raftery, *J. Phys. Chem. C*, **111**, 14579 (2007).
29. X. Yang, Y. Wang, L. Xu, X. Yu and Y. Guo, *J. Phys. Chem. C*, **112**, 11481 (2008).
30. N. C. Saha and H. G. Tompkins, *J. Appl. Phys.*, **72**, 3072 (1992).
31. E. Gyorgy, A. P. Pino, P. Serra and J. L. Morenza, *Surf. Coat. Technol.*, **173**, 265 (2003).
32. I. M. Ismail, B. Abdallah, M. Abou-Kharroub and O. Mrad, *Nucl. Instr. Meth. Phys. Res. B*, **271**, 102 (2012).
33. E. A. Reyes-Garcia, Y. Sun, K. Reyes-Gil and D. Raftery, *J. Phys. Chem. C*, **111**, 2738 (2007).
34. C. D. Valentin, E. Finazzi, G. Pacchioni, A. Selloni, S. Livraghi, M. C. Paganini and E. Giamello, *Chem. Phys.*, **339**, 44 (2007).
35. C. Cantau, T. Pigot, J. C. Dupin and S. Lacombe, *J. Photochem. Photobiol. A Chem.*, **216**, 201 (2010).
36. G. An, W. Ma, Z. Sun, Z. Liu, B. Han, S. Miao, Z. Miao and K. Ding, *Carbon*, **45**, 1795 (2007).
37. H. A. Le, L. T. Linh, S. Chin and J. Jurng, *Powder Technol.*, **225**, 167 (2012).
38. C. H. Wu, *Dyes Pigm.*, **77**, 31 (2008).
39. C. Y. Kuo, *J. Hazard. Mater.*, **163**, 239 (2009).
40. M. Xing, J. Zhang and F. Chen, *Appl. Catal. B: Environ.*, **89**, 563 (2009).
41. N. Daneshvar, D. Salari and A. R. Khataee, *J. Photochem. Photobiol. A: Chem.*, **157**, 111 (2003).